

Realization of Causal Representation Learning to Adjust Confounding Bias in Latent Space

Jia Li¹, Xiang Li², Xiaowei Jia³, Michael Steinbach¹, Vipin Kumar¹

University of Minnesota, ¹ Computer Science and Engineering; ² Bioproducts and Biosystems Engineering.

³ University of Pittsburgh, Computer Science.

¹ {jiaxx213, stei0062, kumar001}@umn.edu, ² lixx5000@umn.edu, ³ xiaowei@pitt.edu

ABSTRACT

Applying Deep Learning (DL) models to graphical causal learning has brought outstanding effectiveness and efficiency but is still far from widespread use in domain sciences. In research of EHR (Electronic Healthcare Records), we realize that some confounding bias inherently exists in the causally formed data, which DL cannot automatically adjust. Trace to the source is because the Acyclic Causal Graph can be *Multi-Dimensional*, so the bias and causal learning happen in two subspaces, which makes it unobservable from the learning process.

This paper initially raises the concept of Dimensionality for causal graphs. In our case, the 3-Dimensional DAG (Directed Acyclic Graph) space is defined by the axes of causal variables, the Absolute timeline, and Relative timelines; This is also the essential difference between *Causality* and *Correlation* problems.

We propose a novel new framework Causal Representation Learning (CRL), to realize Graphical Causal Learning in latent space, which aims to provide general solutions for 1) the inherent bias adjustment and 2) the DL causal models generalization problem. We will also demonstrate the realization of CRL with originally designed architecture and experimentally confirm its feasibility.

KEYWORDS

Causal Representation, Deep Learning, Multi-Dimensional Causality, Higher-Dimensional Feature, Inherent Confounding Bias

1 INTRODUCTION

Graphical causal learning is an important topic for multiple research fields, like meteorology, biology, medicine, epidemiology, social sciences, and policy-making [1–3]. It aims to uncover the underlying causal relationships from observational data, which is naturally generated during the causal process. Better extracted causal information from observations can help us to disentangle questions such as “whether and when the flood will happen”, “what medicines are most effective against complications”, or “what long-term factors determine the population growth in future”.

The study of causality originated from classical statistics, which has developed for decades and contributed greatly to establishing knowledge in many areas. Technological improvement in collecting high-quality data has brought essential challenges to statistical causal analytics: learning graphical causality from data to be Bayesian networks is NP-hard. Meanwhile, machine learning techniques show great potential in causal learning; specifically, it has become a burgeoning topic in the Artificial Intelligence (AI) field as part of bedrock [11].

Conventionally, causal analytics begins with the model specification with prior knowledge, assuming the underlying distributions,

thus may lead to model approximation errors (often called model selection bias in statistics). A great advantage of such classical modeling is to keep it interpretable, thus making it easy to leverage domain knowledge [7]. On the other hand, Deep Learning (DL) applications bring outstanding effectiveness to causal learning. They usually do not require model specifications but reduce modeling approximation errors automatically by optimizing neural network connections. Some recent works greatly enhanced their model efficiency by approximating the discrete structure constraint as a continuous optimization function [4, 20], thus bypassing the NP-hard combinational searching scheme. However, in the meantime, the black-box nature of DL diminishes the modeling interpretability.

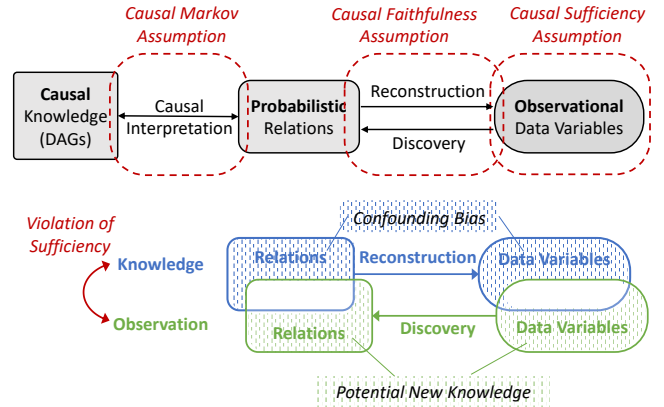


Figure 1: Existing Causal Learning Framework and three Standard Causal Assumptions (referred to in Section 1 & 3.1).

We summarise the current causal learning framework as Fig 1, to describe the processes between what we have known (i.e., Causal Knowledge) and what we can see (i.e., Data Variables). The modeling methods discussed above provide different options for people to realize Causal Discoveries or Reconstructions. Here causal reconstruction refers to the applications of known relations onto observational data, such as estimating causal effects between variables known to be causally related, establishing a synthetic data generator to reflect causal knowledge, and so on. From the modeling perspective, a causal relation equals a correlation with a certain temporal order, which is indistinguishable from the ones ordered in spatial or other ways; and, even further, the ones without order. Since the learning process is throughout a sequence of records whose order matters is not dissimilar to the one without. In other words, the dependencies we learned from the data unnecessarily indicate causal relations but are highly likely to be hybrid, even though the training data is in chronological order. A typical hybrid scenario is with hidden confounders: for a pair of variables, if their

common causes are unobservable, the learned pairwise causation between them can be biased - Such a bias can even “make up” a pseudo correlation when the two are independent of each other. Unfortunately, such a pseudo-relationship can only be identified manually, given prior knowledge. In short, the interpretation process (based on domain knowledge) is indispensable for generating causal relations, which are commonly presented as Directed Acyclic Graphs (DAGs). Thus, it is easy to see that the black-box nature of DL impedes its popularity in domain science applications. The neural networks often provide no meaningful insights into their learned dependencies, although with accurate outputs.

In Fig 1, we did not locate or mark Causal Inference, a classical concept from statistics. While in our opinion, it can be considered as a combination of some manual interpretations (e.g., determining directions of causation) and causal reconstructions (e.g., causal effect estimation).

Recently, some efforts have been made toward interpretable DL models in causal learning. The main principle is to encode the known graphical causal structure among data variables by inferring (part of) the neural network architecture [6]. However, this strategy can hardly achieve general success. It is still very difficult to determine how well the knowledge has been utilized during the networking optimization or why it has not been. Our previous work [9] has confirmed that networking optimization cannot be automatically guided by causal knowledge in some practical occasions, e.g., in EHR (Electronic Healthcare Records) data, some medical effects can be “invisible” to DL models. It can be attributable to some inherent biases existing between Knowledge and Observations, which brings unadjustable confounding bias into DL.

This paper will initially discuss the existence of such a bias (in Section 3.1), named as *Causal Representation Bias (CRB)*. Based on our analysis, the fundamental reason is that the causal graph represented as DAG can be *Multi-Dimensional* due to multiple independent timelines (in Section 3.2). Briefly, the confounding bias and our learning process can happen in distinct subspaces (or planes) of the multi-dimensional DAG, which makes the bias “invisible” to DL models. Furthermore, we will propose a new framework *Causal Representation Learning (CRL)* to be a general solution for the inherent biases adjustment (in Section 3.3); and also demonstrate a realization of CRL (in Section 4) with a proposed novel architecture to extract representations of causal Variables (in Section 4.1-4.2) and causal Effects (in Section 4.3).

Specifically, CRL aims to realize graphical model learning (including reconstruction and discovery) in latent space. For one thing, it can transform causal relations from different spaces into a common one (i.e., the latent feature space) to perform adjustment; For another, it can explicitly preserve the model interpretations in latent space, generally utilizable by DL. It is worth mentioning that the term “CRL” was initially raised in another work [10], where Scholkopf et al. focus on knowledge generalization (making low-level knowledge reusable when learning high-level knowledge) based on certain problems from computer vision field. While this paper aims to broaden this concept as a general framework to provide solutions for the causal DL model generalization problem.

The proposed architecture aims to realize the higher-dimensional representation extraction (in contrast to the traditional lower-dim

one), which is imperative to provide a sufficient degree of freedom for CRL. In the feasibility experiments (in Section 5), we perform the latent-space graphical reconstruction and heuristic discovery on a practical causal learning problem, successfully confirming the effectiveness of the proposed CRL realization method.

In summary, the principal contributions of this paper:

- initially raises Acyclic Causal Graph’s *Multi-Dimensionality*, leading to inherent confounding bias (named CRB) that is not automatically adjustable by DL causal models. It also defines the essential difference between *Causality* and *Correlation* problems.
- summarizes the current causal learning framework, analyzes its limitation, and proposes a new one (CRL) to solve inherent biases and the DL model generalization problem.
- proposes the architecture of higher-dimensional representation extraction to realize CRL and experimentally confirms its feasibility.

2 RELATED WORK

2.1 Representation Learning in Causality

The concept of representation learning was proposed about 100 years ago, including the unsupervised principal component analysis (PCA) in 1901 and supervised linear discriminant analysis (LDA) in 1936. In recent years, the deep network architectures for representation learning have turned out to be widely applied [12]. Data representation describes how much the explanatory factors of variation behind the data have been revealed [13], and thus plays an important role in determining the success of machine learning methods. In the quest for applicable Artificial Intelligence (AI), more powerful methods are motivated to be designed in this direction.

Particularly, for machine learning of causality, the use of representation was raised very recently in the last year [10], where Scholkopf et al. proposed the term “causal representation learning” (CRL), but not mean to concentrate on defining it as a general framework. In this paper, they point out that “most work in causality starts from the premise that the causal variables are given”, and describes three critical challenges we are facing, which also constitute our demands for CRL: 1) The robustness of modeling is still weak; 2) The learned knowledge lacks reusable mechanisms that allow it to be generalized; 3) We do not have effective ways to interpret deep learning results to form new knowledge.

From the probabilistic modeling perspective, the question of causal feature learning (i.e., representation extraction) is to recover a set of latent factors that describe the dependent relations (interpreted as causations) over the observed data variables. For data variable x with latent factor h , their joint distribution can be decomposed as $P(x, h) = P(x|h)P(h)$, where $P(h)$ is a *prior* and $P(x|h)$ is a *likelihood*. Thus a general latent factor model can be inherently interpreted as a latent cause model [13] directed from h to x , denoted as $h \rightarrow x$. This principle forms the basis of the proposed *Causal Representation Learning* to be reasonable.

2.2 Deep Learning in Causality

In recent few years, DL has been applied to realize highly efficient graphical causal models. The key novelty is to turn the discrete possible-DAGs-space searching problem into a smooth function

optimization question [6]. Specifically, these methods quantify the Acyclic-ness of the graph’s adjacency matrix to be a continuous constraint, which established an elegant mathematical connection between the classical combinatorial algorithms and the continuous optimization techniques of machine learning [6]. For instance, Lachapelle et al. described how to convert the DAG learning into a pure neural network learning one in 2019 [5]; and Zheng et al. transformed it into a generalized nonparametric problem that requires no modeling assumptions in 2020 [4].

Based on these realizations, people have made efforts toward the interpretable DL causal models. One way is to figure out conditional independence by finding zero derivatives of the graphical causal functions [5]. Another way is to learn it from the weights of the neural networks [4]: among all Markov causal paths that lead the direction from X to Y , if at least one of them has weight 0, then Y does not depend on X . Such a weights-detecting methodology is also called a Neural Architecture Search (NAS).

As we have confirmed in our previous work [9], DL may not be able to fully utilize the known causal structures in practice, with the inherent obstacle of CRBs. Therefore, the network architecture or weights unnecessarily provide desired interpretations. We propose to leave the interpretation task to be still with conventional models where the knowledge originally come from, and let DL concentrate on representation learning tasks - This strategy is from our newly proposed CRL framework introduced in the next Section.

2.3 Existing Causal Models

Conventionally, the causal models are established on observed data variables. The traditional statistical methods include constraint-based ones and score-based ones. The constraint-based causal discovery, including PC and Fast Causal Inference (FCI), typically detects causation by exploiting conditional independences among data. PC is based on a no-hidden-confounder assumption (equivalent to Causal Sufficiency), while FCI is not. However, there exists a significant deficiency: they can necessarily but not sufficiently identify causations, where the set of possible causal structures satisfying the same conditional independence is called Markov Equivalence Class [8]. The score-based methods usually belong to heuristics. For example, Greedy Equivalence Search (GES) directs its search over the space of equivalence classes using a properly defined score function under the no-hidden-confounder assumption.

The graphical causal models are generated from machine learning, often presented as Functional Causal Models (FCMs) or Structural Equation Models (SEMs) [8]. They assume the value of Y to be a deterministic function of its direct causes X with noise term ϵ , $Y = f(X, \epsilon; \theta)$ where θ indicates the parameters set involved in f . They aim to decompose a causal DAG into a product of simpler factors, where the separation is by conditional independence. It has been shown that they can distinguish different DAGs from an equivalence class and are good at leveraging prior knowledge.

3 CAUSAL REPRESENTATION BIAS

This section will initially raise three relevant terms: Acyclic Causal Graph’s Dimensionality, Causal Representation Bias (CRB), and Causal Representation Learning (CRL).

The multi-dimensionality of the acyclic causal graph is the underlying reason for the inherent confounding bias (CRB). There

exist multiple independent timelines in the causal graph, including the *Absolute* timeline where the causal learning process happens, and the other *Relative* timelines, from where the possibly happened confounding bias is inherently unobservable by causal learning. We will discuss an example in Section 3.2 to illustrate why a causal graph must be in 3-dimensions to stay acyclic; and emphasize that existence of *Relative* timelines fundamentally differentiates the *Causality* problems away from *Correlation* ones.

There may exist multiple relative timelines independent of each other. Hence, the simplest way to solve all possible inherent biases is to transform all causal relations into a common feature space and adjust the confounding biases (maybe) jointly, then the causal learning process can be properly performed in this space. We call this novel framework Causal Representation Learning (CRL).

3.1 Inherent Existence

In statistical analytics, the specified models usually reflect the best guesses from domain scientists about the underlying causality based on the assumption that the variables in observational data can fully represent the model’s variables, denoted as Causal Sufficiency. In other words, it is to assume the consistency between Knowledge and Observations. Fig 1 illustrates two types of its violations: One comes from Observational Limit (Blue-shaded), often presenting as the confounding biases we can be aware of; Another is from Incomplete Knowledge (Green-shaded), which may be reflected as unexplainable biases or other phenomena, potentially containing newly observed relations to form new knowledge.

Since such a confounding bias comes from inappropriate model assumptions, can we conclude that the advanced DL methods, without requiring model specifications, can learn the underlying causality adequately by leveraging prior knowledge? Or, despite interpretation, can they at least provide sufficiently trustable predictions? Here, we emphasize that not all confounding biases can be adjusted as modeling approximation errors. Some inherent biases are “invisible” to the causal learning process and cannot be eliminated by improving the models. However, the required knowledge for adjusting these inherent biases may have been given, the operation of which is out of the scope of the current framework. And that is the motivation for us to reconsider it.

Additionally, unlike Causal Sufficiency, we are usually concerned little about possible violations of the Causal Markov condition (e.g., wrongly inversed causal direction) or Causal Faithfulness assumption (e.g., sampling bias of selecting training data), empirically adjusted in causal learning or interpretation processes.

3.2 Dimensionality of Acyclic Causal Graph

A regular causal relation is often represented as a Directed Acyclic Graph (DAG), which emphasizes “acyclic” to guarantee that any transaction over the variables has to be closed instead of an endless loop. To learn about such a relationship in a regular data matrix with variable values as columns, the learning process usually goes over the rows, i.e., different *Instances*. Particularly, a temporal model (e.g., RNN model) requires properly ordered rows representing the time series and, accordingly, to learn the variables’ value changing along the timeline. Here, an *Instance* often refers to an individual or object with a series of rows describing its temporal changing.

Fig 2 displays two causal relations, where the causal graphs over *Variables* are given at the top, and accordingly, the temporal causal graph of an individual *Instance* is provided below.

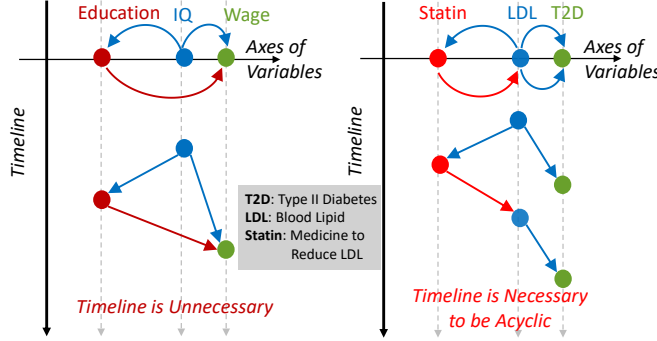


Figure 2: Examples of causal graphs on *Variables*, and correspondingly an individual *Instance* changes its value along the timeline to reflect such a causal relation. (a) Left Side: No need for a timeline to stay Acyclic, equal to a Correlation; (b) Right Side: the Cycle makes the timeline a necessary dimension for constructing a DAG without cycles.

In Fig 2 (a), the temporal learning process going through the rows of all *Instances* in a sequence is equal to a learning process taking each row as an individual *Instance*. In other words, the data rows do not necessarily indicate a timeline but can be assigned any other meaning without changing the model results. So this relation can be seen as equal to a regular *Correlation* without temporal learning. In Fig 2 (b), we can consider the temporarily changing *Instance* to be a patient at risk of diabetes. The causal graph on *Variables* contains cycles because LDL has two values, before and after the patient takes Statin. The probability of getting a T2D diagnosis has also been changed accordingly, forming another cycle. In short, it requires one more dimension, the natural timeline, to construct an acyclic graph. So the *Causality* in (b) is distinguishable from (a).

Furthermore, Fig 2 (b) can also illustrate why there may exist *Causal Representation Bias (CRB)*. In causal learning, the variable LDL may be able to represent its two roles simultaneously, whose difference appears to be the *medical effects*. However, once some confounding bias happens in the Statin-LDL cycle, say, some extra reason makes the no-Statin-taken happen much more times than taking-Statin (which is the usual case in reality), the current LDL values cannot accurately represent its roles but provide biased *medical effects* in the causal learning process.

Commonly, a temporal model goes through time series along the nature timeline and learns the relationship among variables. This process can be seen as on a plane, defined by the axis of all causal variables and the axis of an *Absolute* timeline, where the "absolute" indicates the plane to be fixed and immovable for the current learning task and commonly with nature values. We briefly name this plane as **AT-Plane** and assign the nature dates (in M/D/Y) to be the timeline values in this case (denoted by t).

To construct a DAG for Fig 2 (b), we need to involve an additional axis of a timeline, as shown in Fig 3, which describes how

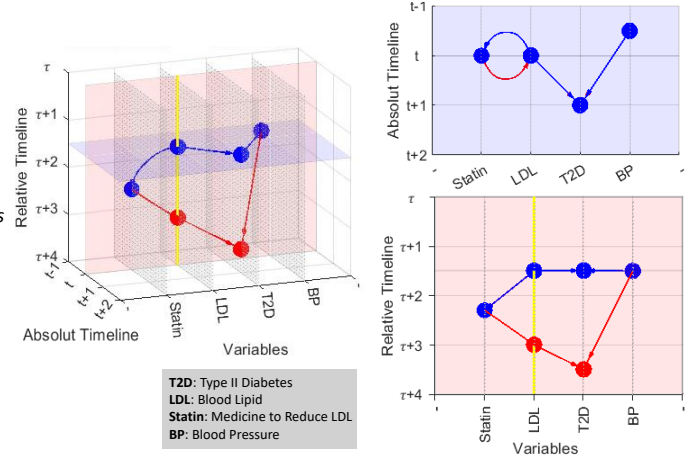


Figure 3: The 3-Dimensional DAG of Fig 2 (b), with one more variable BP. Blue indicates observable in AT-Plane, while red means only observable in RT-Plane. The LDL-Statin cycle is curved for better displaying overlapped edges.

the *medical effects* temporally develops. We name it *Relative* timeline accordingly, and the plane it defines together with the axis of variables is called **RT-Plane**. Notably, such two timelines are independent; in our case, their axes can even be orthogonal.

Specifically, in Fig 2 the two timelines of an instance are different. The one in (a) is *Absolute* one since all instances consistently change their values along it, in other words, this is the timeline to describe *Variables*; While the one in (b) is a *Relative* timeline, which can only be used for an *Instance* that we are interested in, i.e., a patient possibly taking Statin in few days. We intend to emphasize that a *Relative* timeline is for data instances rather than data variables since RT-Plane aims to describe the other *Roles* of the data variables, which cannot be observable in AT-Plane. For example, in Fig 3, the role of LDL-after-taking-Statin can only be seen from the perspective of RT-Plane but not AT-Plane. A pseudo-population has to be concreted to make such a role "visible", in other words, to create a dataset to represent this role specifically. In this case, we must select all instances throughout the data, conditioned as five-day-length segments of the time series (from τ to $\tau + 4$) during which the patient possibly takes Statin.

Therefore, we conclude that learning on RT-Plane has to be *Asynchronous* from the causal learning on AT-Plane, because the dataset it requests is not ready to use but instead initially "scattered" throughout the data. Now, suppose confounding bias exists in RT-Plane, then a pre-processing is required to *Adjust* such a bias on the data to make sure the variables in AT-Plane can properly represent the *Roles*, and subsequently, let the target causal learning be properly performed. Accordingly, we have the definition below.

Definition 1. *Causal Representation Bias (CRB) is Confounding Bias in Relative timeline, whose adjustment has to be Asynchronous from the causal learning process on the Absolute timeline.*

Here we only discussed the scenario of one *Relative* timeline for a typical medical effect. However, various medicines have different effects separately, which may bring multiple RT-Planes on demand

and give the variable multiple independent roles. Particularly, no *Relative* timeline makes *Causality* equivalent to *Correlation*.

Theorem 1. *An Acyclic Causal Graph must have one Absolute timeline and can have multiple independent Relative timelines that make it Multi-Dimensional.*

Here, we initially discuss the causal graph in 3D space but would be very cautious about defining the term *Causal Graph's Dimensionality*. Given the background of EHR data analysis, it seems safe to assume RT-Plans to be orthogonal with the AT-Plane, where the RT-Plans may or may not be mutually parallel (e.g., intersections may indicate associated medical effects). However, many scientific fields with causality concerns have numerous prior knowledge, potentially bringing various possibilities and broader perspectives. Such a multi-dimensionality may come from factors other than timelines (e.g., some spatial factors), lead to more complex plane intersections, or be in higher dimensions like 4D causal graphs or even further. Moreover, the mathematical meaning of multi-dimensional acyclic causal graphs also deserves a lot of exploits.

3.3 Proposed CRL Framework

Under the current causal learning framework (as shown in Fig 1), the existence of CRB can easily be overlooked since it only considers the *Absolute* timeline and focuses on the learning tasks processed along it. This problem is particularly evident in Deep Learning (DL) models. Compared to traditional statistical analytics, DL is more advanced in performance but tends to downplay the interpretation of modeling due to its black-box nature. However, being aware of CRB usually depends on how well the domain knowledge has been applied. To be specific, the known causal relations are required to be identifiable from the model and thereby can be applied to check possible biases. Without any structural interpretation, even though a DL model has occasionally “understood” the given causal knowledge, its generalization will still be a problem.

Another trouble with causal deep learning is that the global optimization strategy brings high efficiency but probably increases the overall biases simultaneously. Unlike traditional heuristics, which can deal with the local confounding bias in each step regardless of other variables, the global DL models wrap up the optimizations of all (pairwise) causations in the graph in one run, possibly letting the local confounding bias impact the global performance.

In recent years, the demands for interpretable causal models significantly boosted cross-disciplinary applications, including the numerous efforts to make domain knowledge utilizable to DL models. However, these efforts are often case-by-case for practical problems and can not be generalized easily. For example, in the previous work [9], we extract a linearly computable estimator to partially adjust confounding bias in medical effects, but with the premise that the known causal structure is luckily to be derivable.

Accordingly, we propose a new framework to realize the generalizable adjustment for the inherent CRBs (as in Fig 4), named as *Causal Representation Learning (CRL)*. The basic principle is to separate the Adjustment and Learning into two individual processes, finished at two different spaces (since for CRB adjustments, they have to be). This way can make DL concentrate on the learning processes at latent space and let the existing causal analytics or knowledge navigate model interpretation. Specifically, we aim

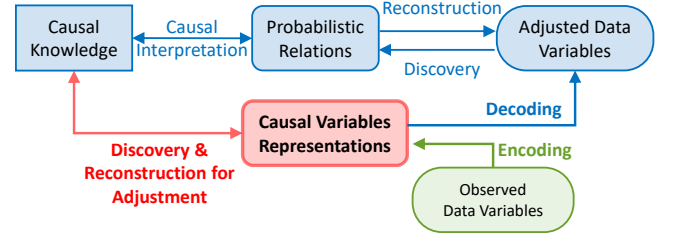


Figure 4: The Proposed Framework: Causal Representation Learning (CRL). Red indicates representation feature space; green is observational data space; and blue means interpretable knowledge space for conventional causal analytics.

to realize an autoencoder to extract the Variable representations individually; then among which the learning tasks (including both causal discoveries and reconstructions) can be performed effectively. In short, we establish Graphical Models in a common latent space to “downgrade” a multi-dimensional causality problem to correlation in it.

On the other hand, such Latent Factor Graphical Models can give DL models explicit structural interpretations in feature space, thus, can be widely used to realize DL model generalization. From an applications perspective, this advantage could be wider useful than CRB adjustment since it also benefits correlations.

4 REALIZATION OF CAUSAL REPRESENTATION

As mentioned in Section 2.1, a general latent factor model $P(x, h)$ can be inherently interpreted as a latent cause model $P(x|h)$. Based on this principle, we can expect reasonably decompose pairwise causation from x to y (denoted as $x \Rightarrow y$) as a causal chain $x \rightarrow h \rightarrow v \rightarrow y$ where v is the latent factor of y , and $x \rightarrow h$ relies on a posterior $P(h|x)$. Such that the dependency between x and y is represented as the posterior distribution $P(v|h)$. Suppose we have the parametrized model $v = f(h)$, then the tuple (v, h, f) can be called a *Representation* of $x \Rightarrow y$ in latent space, consisting of *Variable representations* v and h , and *Effect representation* f .

More importantly, by “stacking” or “splitting” these posterior distributions, we can build up a *Directed Graphical Model* in latent space, which is flexible to be generalized or reused. For example, given causation $x \Rightarrow y \Rightarrow z$, we are interested in the indirect causal effect of x on z , decomposed as $x \rightarrow h \rightarrow v \rightarrow t \rightarrow z$, where t is the latent factor of z , and we want to know $P(t|h) = P(t|v)|_{v=f(h)}$. Since f is known, we only need to learn a conditional *Effect representation* g , such that $t = g(v)|_{v=f(h)}$ by stacking the unknown posterior $P(t|v)$ onto the known posterior $P(v|h)$.

In the following, we will start from the proposed autoencoder architecture for higher-dimensional *Variable representation* extraction (4.1) and the original design of its critical layers (4.2); introduce how to model *Effect representation* in latent space and stack them to realize causal reconstruction (4.3), and heuristic discovery algorithm accordingly (4.4).

4.1 Variable Representation Architecture

The regular autoencoder intends to deal with large-volume objects, like images with numerous pixels, and aims to extract their lower-dimensional features, which is more like a distillation process. However, our appeal is to individually convert causal variables onto latent space, where their dependencies (i.e., causal effects) can be properly modeled. Thus, the common space should be capable of representing all variables, even though they are mutually independent (the worst case of causal learning). Besides, it should provide a sufficient degree of freedom for possibly built causal models, so we must also consider the graphical complexity. For example, in our experimental dataset, lengths of the 10 variables are between 1 ~ 5 and added up to be 32 in total (refer to Table 2); their average node degree will be around 2 ~ 3. Initially, we approximate that 64-dimensional latent space is about to satisfy the requirement, but it turns out to be highly redundant. It is probably because variable attributes are strongly related, and we gradually reduced the dimension to 16. Besides, we envision that refinement or further feature learning can be helpful to make it more efficient.

The biggest challenge to realizing such an autoencoder is extending the input variable vector’s length (i.e., dimensionality), which should sufficiently encode the associative information among its values. More importantly, this process has to be *Invertible*, to achieve high accuracy for the output vector, unlike the regular autoencoders without concern of reconstructing each pixel. We design a pair of layers to finish such two symmetric processes, named *Encrypt* and *Decrypt*, respectively located at the Input and Output of the autoencoder, as shown in Fig 5.

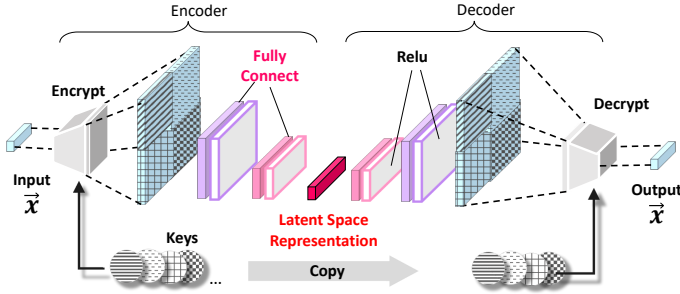


Figure 5: Proposed autoencoder architecture for an individual causal Variable x representation extraction.

The Encrypt works as a “feature amplifier” for extracting higher-order features from the input vector, while Decrypt exactly reverses this process. How much the feature order should reach is on practical demand, such as a *double-wise* amplifying to extract the 2-dimensional associations, or even higher like *triple-wise* to encode 3-dimensional features further. In this work, we only demonstrate the double-wise extraction. To be specific, all possible combinations of two values from this vector will be “encrypted” using a set of constants named *Key*, generated by Encoder. Then the *Key* will be copied by the Decoder to “decrypt” its output back to a pair of such values. For a pair, one *Key* means one time amplifying, so with multiple *Keys*, we can get a group of vectors differently amplified from the same two values; then concatenate them to form a much longer new vector to be a double-wise feature of the input pair of values.

Because for a variable with length n , its double-wise features can be arranged as a $(n - 1) * (n - 1)$ sized matrix, we use a square to represent it in Fig 5 (unnecessarily to be a 2-dimensional feature).

For example, Fig 5 contains four *Keys*, which means extracting four times amplified features. As a metaphor, in this architecture, the role of *Keys* is similar to the filters in a regular autoencoder.

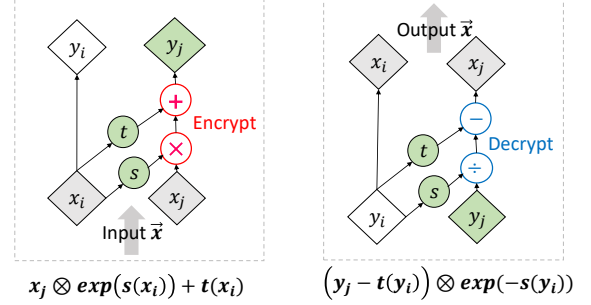


Figure 6: Encrypt and Decrypt with *Key* $\theta = (s, t)$.

4.2 Variable Encrypt and Decrypt

Suppose the input variable denoted as $\vec{X} = (x_1, x_2, \dots, x_n)$ has length n . The Encrypt is defined as a function $f(x_j; x_i, \theta)$, a transformation of x_j using x_i as weights and use the *Key* θ as parameters, where $i \neq j$ and $i, j \in \{1, \dots, n\}$.

Let $\theta = (s, t)$, s.t. $s(x) = w_s x$ and $t(x) = w_t x$, given w_s and w_t . We define that $f(x_j) = x_j \otimes \exp(s(x_i)) + t(x_i)$, where \otimes denotes the element-wise multiplication, and let $y_j = f(x_j)$ to be the corresponding output for x_j . Accordingly, the inversed function f^{-1} in Decrypt is going to be $(y_j - t(y_i)) \otimes \exp(-s(y_i))$. Fig 6 illustrates the two symmetric processes. Because calculation of f^{-1} does not involve inversed function s^{-1} or t^{-1} , the two basic transformation functions s and t can be defined very flexible to be non-linear.

We assemble all f functions as a set $\mathcal{F}(X; \Theta)$, where Θ is the set of all θ . Then the two layers of Encrypt and Decrypt can be denoted as $Y = \mathcal{F}(X; \Theta)$, and $X = \mathcal{F}^{-1}(Y; \Theta)$ respectively. Source codes for these two layers are free for downloading, and the autoencoder realization is also included¹.

We want to highlight that the work of Dinh, L., et al inspires the design above [21]. One can perform higher-order associations by the same principle, like the triple-wise feature extraction.

4.3 Effect Representation and Stacking

Fig 7 displays the architecture of learning the causal Effect representation $h \rightarrow v$ for the causation $x \Rightarrow y$ using the RNN model, which is to construct the causal chain $x \rightarrow h \rightarrow v \rightarrow y$. The feature vectors h and v have been initialized as the extracted Variable representations individually, which have the same dimensionality ($h, v \in \mathcal{R}^L$), but hardly be considered as in a *common feature* space. In this Effect learning process, h and v will keep updated during optimizations to get “closer” to each other. It can be seen that both h and v are shifting in \mathcal{R}^L space toward finding the proper locations minimizing their distance and at the same time letting the RNN sufficiently model their dependence $P(v|h)$, which represents the estimated causal Effect $h \rightarrow v$ in \mathcal{R}^L .

¹https://github.com/kflijia/bijjective_crossing_functions.git

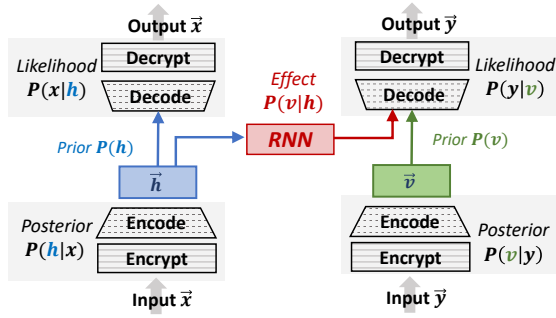


Figure 7: Architecture of learning the RNN model in latent space to build the causal Effect representation $h \rightarrow v$.

There are three optimization tasks with three objective functions respectively, which should be sequentially updated in each iteration:

- (1) Update *posterior* $P(h|x)$ and *likelihood* $P(x|h)$ to minimize the reconstruction error of x .
- (2) Update *posterior* $P(h|x)$ and *Effect posterior* $P(v|h)$ to minimize the reconstruction error of y .
- (3) Update *posterior* $P(v|y)$ and *likelihood* $P(y|v)$ to minimize the reconstruction error of y

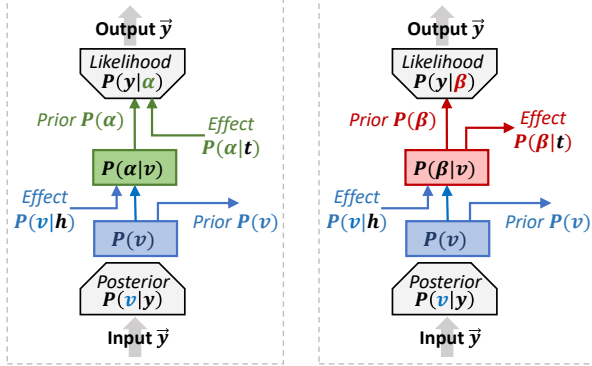


Figure 8: Example of stacking two Causal Representations to fully-connect x, y and z .

“Stacking” two Causal Representations means that given one of them has been well established, we aim to build the second one from either end of the first one to establish a fully-connected 3-nodes causal graph, which can eventually shape as a colliding, a confounding, or a chain. This is essential to ask how to stack two *Effect posteriors*, e.g., stack $P(t|v)$ onto $P(v|h)$ to form the chain $h \rightarrow v \rightarrow t$. There exist four possible occasions by combining two binary options: is the *prior* at the bottom a *cause* or a *result*? And how will the *prior* at the top be?

Suppose y is the data variable whose latent space is where the stacking will happen, and we have x and z at each side of y to be the connecting candidates, presented as the representations h at left and t at right. As shown in Fig 8, the *prior* $P(v)$ at the bottom can be either a *cause* of any other latent factor (output toward the right) or the *result* caused by h (from the input *Effect* $P(v|h)$). While for the top layer, Fig 8 displays two possible roles of t : to be the new *cause* that inputs *Effect* $P(\alpha|t)$ (green colored), or the new *result* that takes output *Effect* $P(\beta|t)$ (red colored). Although with different

directions, in optimization of the top layer, t always represents the fixed *prior* to support updating the *posterior*, $P(\alpha|t)$ or $P(\beta|t)$.

For each occasion, multiple inputs and outputs exist to be the potential entrance and exit, respectively, where the selection would be on demand during causal reconstructions or discoveries. For example, let \mapsto be the notation that connects entrance and exit, then, $P(v|h) \mapsto y$ means output $P(y|x)$, $P(\alpha|t) \mapsto y$ means output $P(y|z)$; $y \mapsto P(\beta|t)$ means output $P(z|y)$ with the ground truth y input, while $P(v|h) \mapsto P(\beta|t)$ means output $P(z|y)|_{y=f(x)}$ where f is the estimated causal effect $x \Rightarrow y$.

From a geometric perspective, the desired common feature space is further specified every time we complete a stacking in \mathcal{R}^L . Suppose L is large enough to provide a sufficient degree of freedom throughout the causal graph. In that case, we can finally obtain a group of feature vectors in \mathcal{R}^L , which have been optimized to distribute as tight as possible, prepared for further processes, such as dimensionality reduction, feature learning, and so on.

4.4 Discovery Algorithm in Latent Space

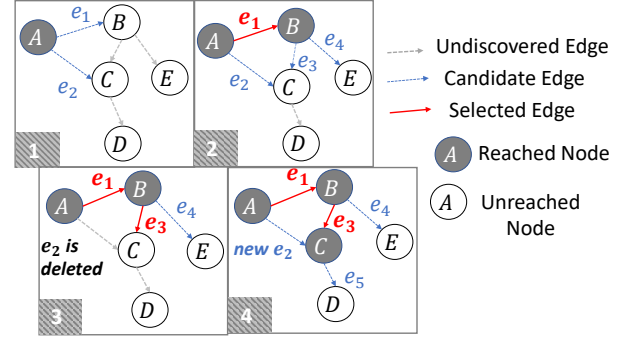


Figure 9: Example of Causal Discovery in feature space. Nodes indicate the variable representations or latent factors.

Here we adopt heuristics to realize causal discovery in latent space among Variable representations, using KLD (KL-Divergence) as the metric to evaluate the similarity between two feature vectors in the common latent space \mathcal{R}^L , as shown in Algorithm 1. The conventional MSE evaluation can also be considered. However, it has been realized that the MSE-based optimization subject to acyclicity constraint has some inherent restrictions and may mislead the model to be dominated by data variance instead of causality [18, 19].

An illustrative example is given in Fig 9. In the four consecutive steps, edge e_1 and edge e_3 are selected one after another, since the selected e_1 make node B reachable, and B is the start node of e_3 . At step 3, the learned causal effect of e_2 , from A to C, is deleted from the candidate edges and need to be recalculated, because edge e_3 has reached C and changed the causal conditions on C.

5 FEASIBILITY EXPERIMENTS

The feasibility experiments aim to confirm that: 1) the proposed autoencoder with *Encrypt* and *Decrypt* can effectively extract higher-dimensional causal variable representations. 2) the causal effects can be successfully represented in latent space and used to complete graphical causal reconstructions. 3) the heuristic causal discovery can effectively work in latent space.

Algorithm 1: Causal Discovery with KLD Metric

```

Result: ordered edges set  $E = \{e_1, \dots, e_n\}$ 
 $E = \{\}$ ;
 $N_R = \{n_0 \mid n_0 \in N, \text{Parent}(n_0) = \emptyset\}$ ;
while  $N_R \subset N$  do
   $\Delta = \{\}$ ;
  for  $n \in N$  do
    for  $p \in \text{Parent}(n)$  do
      if  $n \notin N_R$  and  $p \in N_R$  then
         $e = (p, n)$ ;
         $\beta = \{\}$ ;
        for  $r \in N_R$  do
          if  $r \in \text{Parent}(n)$  and  $r \neq p$  then
             $\beta = \beta \cup r$ 
          end
        end
         $\delta_e = K(\beta \cup p, n) - K(\beta, n)$ ;
         $\Delta = \Delta \cup \delta_e$ ;
      end
    end
  end
   $\sigma = \text{argmin}_e(\delta_e \mid \delta_e \in \Delta)$ ;
   $E = E \cup \sigma$ ;
   $N_R = N_R \cup n_\sigma$ ;
end

```

$G = (N, E)$	graph G consists of nodes set N and edges set E
N_R	the set of reachable nodes
E	edges in order of being discovered
$K(\beta, n)$	KLD metric between the causes set β and effect node n
$\Delta = \{\delta_e\}$	the set of all KLD Gain δ_e for each candidate edge e
n, p, r	notation of node
e, σ	notation of edge

Our experiments are performed on a professionally calibrated synthetic hydrology dataset generated by SWAT (Soil & Water Assessment Tool), a commonly used hydrology data simulation system based on physical modules. These physical models are jointly connected to form a causal graph. The question from the hydrology domain is that the models learned from nearby watersheds can hardly share their learned knowledge because existing physical methods lack generalizability. The next experiment on this data will be toward a practically effective model-generalization method.

However, this problem belongs to correlation but not necessarily to causality. Due to some empirical restrictions, in this work, we do not have EHR data to verify how well it works on CRB adjustment, but that would be our immediate next move.

5.1 Hydrology Dataset

The hydrology system entails water fluxes and states across the earth’s space, such as snowpack melting, evapotranspiration, and soil moisture. The underlying hydrologic processes are highly complex, exhibit nonlinearities, and contain a lot of unobservable dependencies. In recent years machine learning on causal inferences naturally attracted hydrologists’ attention [14]; Also, DL-based methods are widely used to extract representations from time series efficiently. As a typical application, RNN models contribute state-of-the-art techniques for streamflow prediction [15–17].

Streamflow is a critical state variable in hydrologic processes, where the hydrologists attempted to explain the causal relationship between observable environmental variables and the subsequential streamflow records, but have not achieved a satisfying performance.

Table 1: Nodes in Fig 10 Hydrology Causal Graph

ID	Variable Name	Interpretation
A	Conditions Part I	Wind Speed + Humidity + Temperature
B	Conditions Part II	Temperature + Solar Radiation + Precipitation
C	Evapotranspiration	Evaporation and transpiration
D	Snowpack	The winter frozen water in the ice form
E	Soil Water	Soil moisture in vadose zone
F	Aquifer	Groundwater storage
G	Surface Runoff	Flowing water over the land surface
H	Lateral	Vadose zone flow
I	Baseflow	groundwater discharge
J	Streamflow	Surface runoff + lateral flow + baseflow

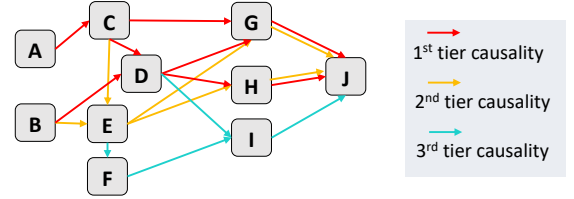


Figure 10: The Underlying Causal Graph from domain knowledge with different causality strengths.

Our experiments are based on such a prediction task, using synthetic data generated by SWAT system, which simulates the Root River Headwater watershed in Southeast Minnesota. From this dataset, we adopted the time series that lasts 60 virtual years, in a daily update frequency, to be the unsupervised training samples.

Fig 10 displays the hypothesized graphical causality assumed in SWAT. Explanations about the nodes in graph are listed in Table 1. Hydrologic processes present different levels of contributions. Surface runoff generation processes (1st tier causality) cause streamflow peak more easily than lateral flow generation processes (2nd tier causality), which are more important than baseflow dynamics (3rd tier causality). For convenience, they are represented by different colors.

5.2 Experimental Results of Causal Variable Representation Extraction

The proposed causal Variable representation extraction method is performed sequentially on each node of the causal graph, from A to J. The challenges of these tasks come from the low dimensionality of variables. As shown in Table 2, the number of attribute columns maximally reaches 5, and the predictive target node J, i.e., Streamflow, is just a one-column variable.

We firstly expand the attributes of each node to a uniform larger count of 12 by randomly repeating their columns, then augmented with 12-dimensional dummy variables of months to form a 24-dimensional input layer. In the 24 double-wise feature amplifications, every column has been extracted 23 times, augmented with the original vector. This way, we have a 576-dimensional output space through *Enrypt* process. In our experimental context, the feature space for representations is set to be 16-dimensional.

Table 2 shows each node’s statistics characteristics and the RMSE Evaluation between the Output and Input of the autoencoder, where

Table 2: Performance of Autoencoder (Causal Variables Representation).

Nodes	# Column	Mean	Std	Min	Max	Non-Zero Rate%	RMSE On Scaled	RMSE On Original	BCE On Mask
A	5	1.8513	1.5496	-3.3557	7.6809	87.54	0.093	0.871	0.095
B	4	0.7687	1.1353	-3.3557	5.9710	64.52	0.076	0.678	1.132
C	2	1.0342	1.0025	0.0	6.2145	94.42	0.037	0.089	0.428
D	3	0.0458	0.2005	0.0	5.2434	11.40	0.015	0.679	0.445
E	2	3.1449	1.0000	0.0285	5.0916	100	0.058	3.343	0.643
F	4	0.3922	0.8962	0.0	8.6122	59.08	0.326	7.178	2.045
G	4	0.7180	1.1064	0.0	8.2551	47.87	0.045	0.81	1.327
H	4	0.7344	1.0193	0.0	7.6350	49.93	0.045	0.009	1.345
I	3	0.1432	0.6137	0.0	8.3880	21.66	0.035	0.009	1.672
J	1	0.0410	0.2000	0.0	7.8903	21.75	0.007	0.098	1.088

Table 3: Brief Results of Heuristic Discovery: the edges in detected order and their measured causal strengths.

Edge	A \Rightarrow C	B \Rightarrow D	C \Rightarrow D	C \Rightarrow G	D \Rightarrow G	G \Rightarrow J	D \Rightarrow H	H \Rightarrow J	B \Rightarrow E	E \Rightarrow G	E \Rightarrow H	C \Rightarrow E	E \Rightarrow F	F \Rightarrow I	I \Rightarrow J	D \Rightarrow I
KLD	7.63	8.51	10.14	11.60	27.87	5.29	25.19	15.93	37.07	39.13	39.88	46.58	53.68	45.64	17.41	75.57
Gain	7.63	8.51	1.135	11.60	2.454	5.29	25.19	0.209	37.07	-5.91	-3.29	2.677	53.68	45.64	0.028	3.384

less RMSE indicates lower information loss; in other words, the proposed autoencoder architecture is more effectively extracted the causal variable’s representation. We provide two RMSE evaluations for the nodes in the scaled (i.e., normalized) and original values, respectively. Besides, the characteristic columns, including Mean, Std, Min, and Max, are calculated at the scaled values.

It is worth mentioning that the hydrology dataset contains a large number of meaningful zero values. For example, the variable of node *D*, named Snowpack, only has non-zero values in winter, whose water body will present as Soil Water in the other seasons. However, the zeros do have meanings since they represent the variables vanishing. Therefore, we perform double reconstructions simultaneously in autoencoder: one for the real value and the other for the non-zero indicator (accessed by BCE), named Mask. The RMSE performances in Table 2 are obtained by multiplying these two results. The percentage of non-zero values is also provided for each node. These very low RMSE values indicate the success of the reconstruction processes, which are in the range of [0.01, 0.09], except node *F*, the Aquifer variable. It has been known that the aquifer system modeling is still premature in the present hydrology area. So this is reasonable to infer that in the synthetic data, Aquifer is closer to random noise than other variables.

5.3 Experimental Results of Causal Effect Representation and Reconstruction

The causal effect representation learning in latent space is evaluated on each pairwise causation. Then, by stacking them, we successfully reconstruct the graphical causal structure shown in Fig 10. For evaluating the performances of these stacking processes, say whether they can enhance the causal effect of the *result* node, we make such performance comparisons from the view of every single node, to be as the effected *result* node in a causal relation, as listed in Table 4. For example, node *G* has three possible causes *C*, *D*, and *E*. Thus we can build up four models in total: the effect estimation of each pairwise causation without stacking, including $C \Rightarrow G$, $D \Rightarrow G$, $E \Rightarrow G$, and the effect estimation as in the fully reconstructed graphical models, which is $CDE \Rightarrow G$. For convenience, we call them the *pairwise-effect* and *stacking-effect*, respectively.

Additionally, in Table 4 we also display the initial performance of each node, i.e., its autoencoder performance before learning any causal effects, to be the baseline comparison, named as “Variable Representation (Before Effect Learning)” in the table.

There are three different optimization tasks in the causal effect representation learning process (refer to Section 4.3), among which both the *second* and *third* one are about the *result* node. Therefore, in Table 4 we give out the performances of these two roles for each node: the role in the *third* optimization is shown as the columns named “Variable Representation (After Effect Learning)”; and the role of the *second* one is in the columns named “Causal Effect Representation”, which represent the effect learning performances of RNN models, along with the KLD metrics to present learned causal strengthened.

By observations, the KLD metric differences in causal strength are easy to see. Node *J* has the smallest KLD values, which means that node *G* (Surface Runoff), *H* (Lateral), and *I* (Baseflow) significantly cause *J* (Streamflow). While the weak causal relations present as high values of KLD. For example, node *I* can hardly be predictable given *D* and *F*. For *result* nodes, *D*, *E*, *J*, the *stacking-effect* causal strength is in the intermediate range of *pairwise-effect* strength, which implies that the associative relationships among their causes nodes are ambiguous. For *G* and *H*, the *stacking-effect* causal strength KLD is lower than all the *pairwise-effect* ones. It is reasonable to infer that the *stacking-effect* model has captured additional causal information from the associative relationships among their causes nodes. Besides, the KLD metric also tells which cause node contributes the most to this causal effect. For example, $C \Rightarrow G$ strength is closer to $CDE \Rightarrow G$ than the other causes nodes, which indicates *C* to be the strongest source in this causal effect.

To better present the Causal Graph Structure Reconstruction performance, we use these reconstructed models as a data simulator and show their simulation results as in Fig 11, which displays three different nodes, *J*, *G*, and *I* in a same synthetic year. For each node, the initial variable representation performance (i.e., the autoencoder performance before effects learning) is plotted as the blue line, and all the causal effects we have learned are displayed in

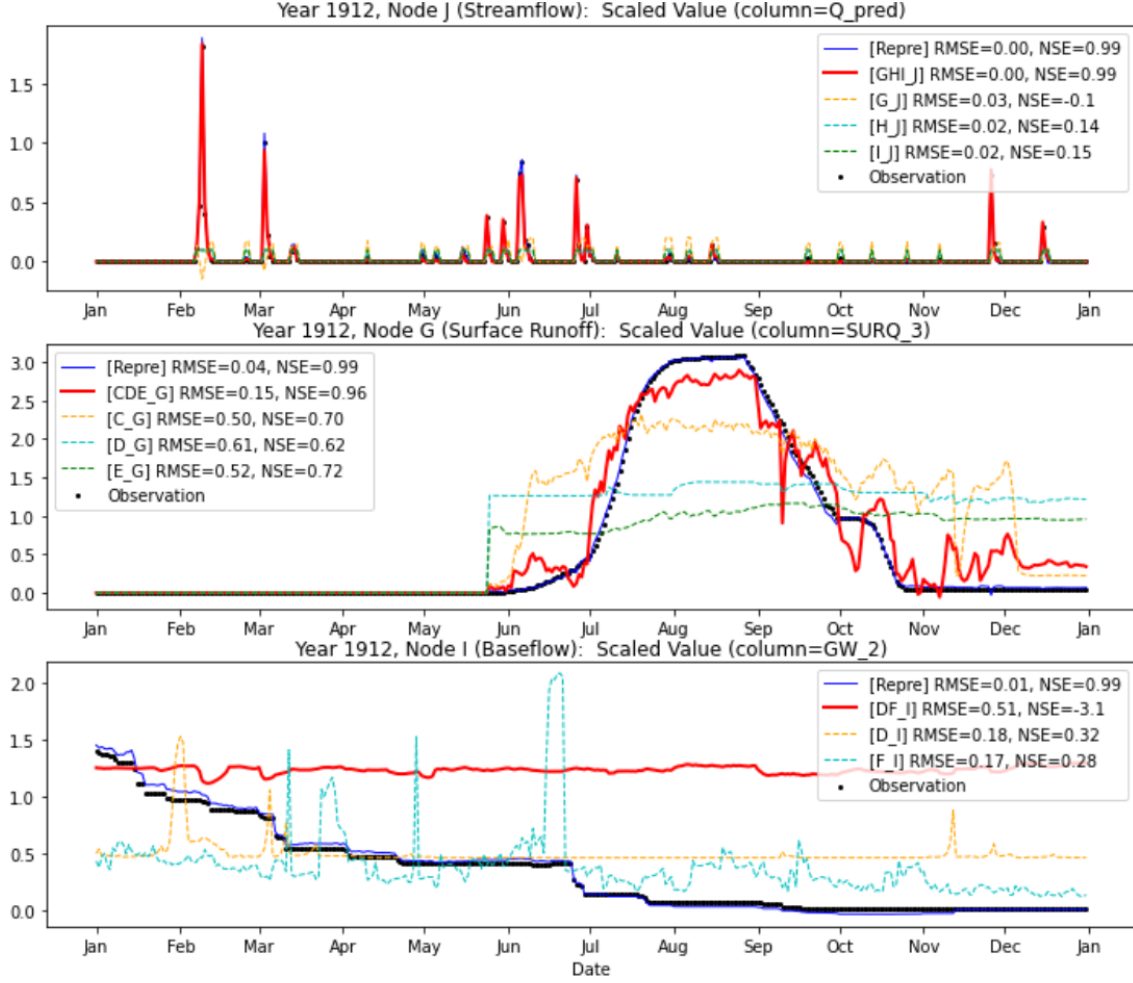


Figure 11: Causal Graphical Structure Reconstruction Performance Comparison (data simulations)

different colors. Besides RMSE, here we also adopted a hydrology-using metric NSE (Nash–Sutcliffe model efficiency coefficient) to assess predictive accuracy, where $NSE = 1$ defines the best prediction. The three initial variable representations (blue line) in Fig 11 almost reach the best performance, as they overlapped with the ground truth observations (black dots). The red line represents the simulations from *stacking-effect*, whose performances are highly consistent with our analysis above: Node *J* has the best prediction; node *I* can hardly be predictable; and node *G* is predicted best by *CDE* causes combination, where *C* provides the strongest causality.

5.4 Experimental Results of Causal Discovery

The discovery heuristic process is based on the KLD causal strength. 3 shows the edges' discovered order and the corresponding KLD and KLD-Gain. Here the table cells are colored according to different tiers of causality, i.e., the ground truth of causal strengths, as displayed in Fig 10. Since the discovery algorithm successfully distinguished different causality strength levels, the proposed KLD metric is confirmed effective.

Due to limited space, the result in Table 3 is a brief version, while the complete one is provided in Appendix A Table 1, which includes

all results in each detecting round and the corresponding decision-making. We also performed the conventional FGES (Fast Greedy Equivalence Search) causal discovery in 10 cross-validation, which is worse than our method, given in Appendix A Table 2.

6 CONCLUSION

In this paper, we initially discussed the concept of Multi-Dimensionality for Acyclic Causal Graphs. It is the fundamental reason for inherent confounding biases of causal learning, which we first named Causal Representation Bias (CRB). In our opinion, this is also where the difficulties of applying the Deep Learning models in causality stem from. Because CRB cannot be eliminated from causal learning by reducing the modeling approximation error; On the contrary, the highly efficient global optimization strategy with continuous constraint may increase the influence of CRB.

In the discussed scenario, the 3-Dimensional space of DAG is defined by the axes of the causal variables, the Absolute timeline where the causal learning happens, and Relative timelines where the CRB possibly happens. We accordingly proposed a novel new framework Causal Representation Learning (CRL), which is to realize graphical models in latent space, such that 1) all causal relations

Table 4: The latent-space causal effect representations learning performances.

Effect Node	Variable Representation (Before Effect Learning)			Causes Node(s)	Variable Representation (After Effect Learning)			Causal Effect Representation			
	RMSE		BCE Mask		RMSE		BCE Mask	RMSE		BCE Mask	KLD In Feature Space
	On Scaled Values	On Original Values			On Scaled Values	On Original Values		On Scaled Values	On Original Values		
C	0.037	0.089	0.428	A	0.0295	0.0616	0.4278	0.1747	0.3334	0.4278	7.6353
D	0.015	0.679	0.445	BC	0.0350	1.0179	0.1355	0.0509	1.7059	0.1285	9.6502
				B	0.0341	1.0361	0.1693	0.0516	1.7737	0.1925	8.5147
				C	0.0331	0.9818	0.3404	0.0512	1.7265	0.3667	10.149
E	0.058	3.343	0.643	BC	0.4612	26.605	0.6427	0.7827	45.149	0.6427	39.750
				B	0.6428	37.076	0.6427	0.8209	47.353	0.6427	37.072
				C	0.5212	30.065	1.2854	0.7939	45.791	1.2854	46.587
F	0.326	7.178	2.045	E	0.4334	8.3807	3.0895	0.4509	5.9553	3.0895	53.680
G	0.045	0.81	1.327	CDE	0.0538	0.9598	0.0878	0.1719	3.5736	0.1340	8.1360
				C	0.1057	1.4219	0.1078	0.2996	4.6278	0.1362	11.601
				D	0.1773	3.6083	0.1842	0.4112	8.0841	0.2228	27.879
				E	0.1949	4.7124	0.1482	0.5564	10.852	0.1877	39.133
H	0.045	0.009	1.345	DE	0.0889	0.0099	2.5980	0.3564	0.0096	2.5980	21.905
				D	0.0878	0.0104	0.0911	0.4301	0.0095	0.0911	25.198
				E	0.1162	0.0105	0.1482	0.5168	0.0097	3.8514	39.886
I	0.035	0.009	1.672	DF	0.0600	0.0103	3.4493	0.1158	0.0099	3.4493	49.033
				D	0.1212	0.0108	3.0048	0.2073	0.0108	3.0048	75.577
				F	0.0540	0.0102	3.4493	0.0948	0.0098	3.4493	45.648
J	0.007	0.098	1.088	GHI	0.0052	0.0742	0.2593	0.0090	0.1269	0.2937	5.5300
				G	0.0077	0.1085	0.4009	0.0099	0.1390	0.4375	5.2924
				H	0.0159	0.2239	0.4584	0.0393	0.5520	0.4938	15.930
				I	0.0308	0.4328	0.3818	0.0397	0.5564	0.3954	17.410

from the DAG can be transformed onto a common space to realize CRB adjustment and de-confounded causal modeling; 2) the model interpretability can be preserved in the latent space to realize Deep Learning causal models' generalization.

We also proposed a novel deep network architecture (with the originally designed layers Encrypt and Decrypt) to realize CRL and experimentally confirmed its feasibility.

CRL provides a new perspective on causal learning and raises many valuable questions as well as forward directions, like the meaning of causal graph dimensionality, feature explanation in the latent learning space, and so on; From the aspect of applications, like complex medical effects estimation, non-model-based causal simulation, and so on. We expect a flourishing development can happen in the following years.

REFERENCES

- [1] Wood, Christopher J., and Robert W. Spekkens. *The lesson of causal discovery algorithms for quantum correlations: Causal explanations of Bell-inequality violations require fine-tuning*. New Journal of Physics 17.3 (2015): 033002.
- [2] Vuković, Matej, and Stefan Thalmann. *Causal Discovery in Manufacturing: A Structured Literature Review*. Journal of Manufacturing and Materials Processing 6.1 (2022): 10.
- [3] Ombadi, Mohammed, et al. *Evaluation of methods for causal discovery in hydrometeorological systems*. Water Resources Research 56.7 (2020): e2020WR027251.
- [4] Zheng, Xun, et al. *Learning sparse nonparametric dags*. International Conference on Artificial Intelligence and Statistics. PMLR, 2020.
- [5] Lachapelle, Sébastien, et al. *Gradient-based neural dag learning*. arXiv preprint arXiv:1906.02226 (2019).
- [6] Luo, Yunan, Jian Peng, and Jianzhu Ma. *When causal inference meets deep learning*. Nature Machine Intelligence 2.8 (2020): 426-427.
- [7] Sobel, Michael E. *An introduction to causal inference*. Sociological Methods & Research 24.3 (1996): 353-379.
- [8] Glymour, Clark, Kun Zhang, and Peter Spirtes. *Review of causal discovery methods based on graphical models*. Frontiers in genetics 10 (2019): 524.
- [9] Li, Jia, et al. *Teaching deep learning causal effects improves predictive performance*. arXiv preprint arXiv:2011.05466 (2020).
- [10] Schölkopf, Bernhard, et al. *Toward causal representation learning*. Proceedings of the IEEE 109.5 (2021): 612-634.
- [11] Li, Yunzhu, et al. *Causal discovery in physical systems from videos*. Advances in Neural Information Processing Systems 33 (2020): 9180-9192.
- [12] Zhong, Guoqiang, et al. *An overview on data representation learning: From traditional feature learning to recent deep learning*. The Journal of Finance and Data Science 2.4 (2016): 265-278.
- [13] Bengio, Yoshua, Aaron C. Courville, and Pascal Vincent. *Unsupervised feature learning and deep learning: A review and new perspectives*. CoRR, abs/1206.5538 1.2665 (2012): 2012.
- [14] Goodwell, Allison E., et al. *Debates—Does information theory provide a new paradigm for Earth science? Causality, interaction, and feedback*. Water Resources Research 56.2 (2020): e2019WR024940.
- [15] Kratzert, Frederik, et al. *Rainfall-runoff modeling using long short-term memory (LSTM) networks*. Hydrology and Earth System Sciences 22.11 (2018): 6005-6022.
- [16] Kratzert, Frederik, et al. *Towards learning universal, regional, and local hydrological behaviors via machine learning applied to large-sample datasets*. Hydrology and Earth System Sciences 23.12 (2019): 5089-5110.
- [17] Li, Xiaojie, Jian Tang, and Chengxiang Yin. *Sequence-to-Sequence Learning for Prediction of Soil Temperature and Moisture*. IEEE Geoscience and Remote Sensing Letters 19 (2022): 1-5.
- [18] Reisach, Alexander G., Christof Seiler, and Sebastian Weichwald. *Beware of the simulated dag! varsortability in additive noise models*. arXiv preprint arXiv:2102.13647 (2021).
- [19] Kaiser, Marcus, and Maksim Sipos. *Unsuitability of NOTEARS for causal graph discovery*. arXiv preprint arXiv:2104.05441 (2021).
- [20] Zheng, Xun, et al. *Dags with no tears: Continuous optimization for structure learning*. Advances in Neural Information Processing Systems 31 (2018).
- [21] Dinh, Laurent, Jascha Sohl-Dickstein, and Samy Bengio. *Density estimation using real nvp*. arXiv preprint arXiv:1605.08803 (2016).

Appendix A COMPLETE EXPERIMENTAL RESULTS OF CAUSAL DISCOVERY

Table 2: Average performance of 10-Fold FGES (Fast Greedy Equivalence Search) causal discovery, with the prior knowledge that each node can only cause the other nodes with the same or greater depth with it. An edge means connecting two attributes from two different nodes, respectively. Thus, the number of possible edges between two nodes is the multiplication of the numbers of their attributes, i.e., the lengths of their data vectors.
(All experiments are performed with 6 different Independent-Test kernels, including chi-square-test, d-sep-test, prob-test, disc-bic-test, fisher-z-test, mvplr-test. But their results turn out to be identical.)

Cause Node	A	B	C		D			E		F	G	H	I
True Causation	$A \rightarrow C$	$B \rightarrow D$	$C \rightarrow D$	$C \rightarrow E$	$C \rightarrow G$	$D \rightarrow G$	$D \rightarrow H$	$D \rightarrow I$	$E \rightarrow F$	$E \rightarrow G$	$E \rightarrow H$	$F \rightarrow I$	$H \rightarrow J$
Number of Edges	16	24	6	4	8	12	12	9	8	8	8	12	4
Probability of Missing	0.038889	0.125	0.062	0.06875	0.039286	0.069048	0.2	0.142857	0.3	0.003571	0.2	0.142857	0.072727
Wrong Causation			$C \rightarrow F$				$D \rightarrow E$	$D \rightarrow F$				$F \rightarrow G$	$G \rightarrow H$
Times of Wrongly Discovered			5.6				1.2	0.8				5.0	8.2
												$H \rightarrow I$	$I \rightarrow J$
												3.0	2.8
												0.0	0.030303

Table 3: Brief Results of the Heuristic Causal Discovery in latent space, identical with Table 3 in the paper body, for better comparison to the traditional FGES methods results on this page.

The edges are arranged in detected order (from left to right) and their measured causal strengths in each step are shown below correspondingly.

Causal strength is measured by KLD values (less is stronger). Each round of detection is pursuing the least KLD gain globally. All evaluations are in 4-Fold validation average values. Different colors represent the ground truth causality strength tiers (referred to the Figure 10 in the paper body).

Causation	$A \rightarrow C$	$B \rightarrow D$	$C \rightarrow D$	$C \rightarrow G$	$D \rightarrow G$	$G \rightarrow J$	$D \rightarrow H$	$H \rightarrow J$	$C \rightarrow E$	$B \rightarrow E$	$E \rightarrow G$	$E \rightarrow H$	$E \rightarrow F$	$F \rightarrow I$	$I \rightarrow J$	$D \rightarrow I$
KLD	7.63	8.51	10.14	11.60	27.87	5.29	25.19	15.93	46.58	65.93	39.13	39.88	53.68	45.64	17.41	75.57
Gain	7.63	8.51	1.135	11.60	2.454	5.29	25.19	0.209	46.58	-6.84	-5.91	-3.29	53.68	45.64	0.028	3.384